^1H and ^{15}N Magnetic Resonance Assignments, Secondary Structure, and Tertiary Fold of *Escherichia coli* DnaJ(1−78)†

R. Blake Hill,‡ John M. Flanagan,*,§ and James H. Prestegard*,‡

Department of Chemistry, Yale University, New Haven, Connecticut 06520, and Department of Biology, Brookhaven National Laboratory, Upton, New York 11973

Received October 21, 1994; Revised Manuscript Received February 13, 1995⊗

ABSTRACT: We report the ^1H and ^{15}N chemical shift assignments along with an NMR-derived preliminary structure for DnaJ(1−78), a highly conserved N-terminal domain of DnaJ, the *Escherichia coli* Hsp40 homolog. This 9 kDa domain is believed to cooperate with DnaK, the *E. coli* Hsp70 homolog, in regulating a variety of cellular functions. Heteronuclear 3D NMR experiments were carried out on a uniformly ^{15}N-labeled DnaJ(1−78), which is a stable, folded fragment. Standard ^{15}N-edited NMR techniques afforded complete assignment of the backbone amide ^1H and ^{15}N pairs and partial assignment of the side-chain ^1H and ^{15}N atoms. The secondary structure of DnaJ(1−78) was determined from NOE connectivities obtained from 3D ^{15}N-separated and 2D homonuclear NOESY spectra as well as $^3J_{HNH\alpha}$ coupling constants obtained from a DQF-COSY spectrum and a ^{15}N-edited HNHA experiment. The stability of secondary structural elements was assessed by monitoring amide exchange rates, and a model for the three-dimensional fold of these elements was derived from a set of long-range contacts extracted from homonuclear 2D NOESY experiments. The analysis indicates that DnaJ(1−78) is comprised of four α-helices and no β-sheet with a short unstructured loop between antiparallel helices II and III. The shorter N-terminal and C-terminal helices make contacts with helices II and III at points well removed from the central loop. A discussion of how this preliminary structural model may explain mutation data from other laboratories is presented.

The *Escherichia coli* Hsp40[1] chaperone, DnaJ, interacts with DnaK (Hsp70) and through these interactions helps to control a plethora of cellular processes including transcription, translocation, and protein folding (Bork et al., 1992; Caplan et al., 1993; Georgopoulos, 1992; Georgopoulos & Welch, 1993; Hartl et al., 1994; Kelley & Georgopoulos, 1992; McKay, 1993; Silver & Way, 1993; Srivastava, 1993; Stuart et al., 1994; Winfield & Jarjour, 1991). Homologs of this Hsp40 chaperone have been discovered in many eukaryotes including humans (Cheetham et al., 1992), and recent work has started to elucidate the mechanisms of Hsp40's interaction with Hsp70 in these various processes. In each case, DnaJ, or its homolog, stimulates upon interaction the ATPase activity of DnaK, or its homolog (Caplan et al., 1993; Feldheim et al., 1992; Hendrick et al., 1993; Langer et al., 1992; Rowley et al., 1994). The exact nature of this Hsp40/Hsp70 cooperation on the atomic level is unknown, although a high-resolution structure of the ATPase domain of the bovine Hsp70 has been determined by X-ray crystallographic methods (Flaherty et al., 1990). We seek to supplement this information with structural data on DnaJ, which may serve as a foundation for a better understanding of these protein−protein interactions.

DnaJ is a basic, dimeric protein with a molecular mass of 43 kDa per monomer (Bardwell et al., 1986; Zylicz et al., 1985). It is a modular protein comprised of at least four distinct functional and structural domains (Bork et al., 1992; Caplan et al., 1993; Silver & Way, 1993). The ATPase stimulatory activity of DnaJ has been shown to reside in the N-terminal 104 residues of the protein (Szabo et al., 1994; Wall et al., 1994), and the first 70−80 residues constitute the most highly conserved module of the protein, which has been termed the "J-homology" domain (Caplan et al., 1993; Georgopoulos & Welch, 1993; Kelley & Georgopoulos, 1992; Stuart et al., 1994). Some Hsp40 homologs are related to *E. coli* DnaJ only by the presence of the J-homology region and are still capable of interacting with a Hsp70 homolog. Also, several point mutations resulting in the loss of cooperativity between Hsp70 and Hsp40 have been mapped to the J-homology domain (Feldheim et al., 1992; Nelson et al., 1993; Wall et al., 1994). It is noteworthy that there are no known point mutations outside this region that affect this interaction. These studies suggest that the J-homology region of DnaJ is responsible, in part, for

† This work was supported by U.S. Public Health Service Grants GM32243 and GM39546, Brookhaven National Laboratory Directed Research and Development Program No. 93-32, and instrumentation provided by the NSF, DIR 9015967. R.B.H. acknowledges the Heyl Foundation for generous support.

‡ Yale University.

§ Brookhaven National Laboratory.

⊗ Abstract published in *Advance ACS Abstracts,* April 1, 1995.

[1] Abbreviations: ADP, adenosine 5′-diphosphate; ATP, adenosine 5′-triphosphate; CD, circular dichroism spectroscopy; DANTE, *d*elays *a*lternating with *n*utations for *t*ailored *e*xcitation; DIPSI-2, *d*ecoupling *i*n the *p*resence of *s*calar *i*nteractions; DQF-COSY, double-quantum-filtered correlation spectroscopy; EDTA, ethylenediaminetetraacetic acid; GE, gradient-enhanced spectroscopy; GSE, gradient sensitivity enhanced spectroscopy; HLA, human leukocyte antigen; HMQC, heteronuclear multiple-quantum correlation; HNHA, intraresidue, backbone amide proton-α proton correlation; HOHAHA, homonuclear Hartmann−Hahn correlation; Hsp, heat shock protein; HSQC, heteronuclear single-quantum coherence; MHC, major histocompatibility complex; NMR, nuclear magnetic resonance spectroscopy; NOE, nuclear Overhauser effect; NOESY, NOE spectroscopy; PCR, polymerase chain reaction; PMSF, phenylmethanesulfonyl fluoride; TPPI, time-proportional phase incrementation; Tris, tris(hydroxymethyl)-aminomethane; TSP, 3-(trimethylsilyl)tetradeuteriopropionic acid sodium salt; 2D, two dimensional; 3D, three dimensional; $^3J_{HNH\alpha}$, three bond, backbone amide proton−α proton coupling constant.

0006-2960/95/0434-5587$09.00/0

mediating the interaction between DnaJ and DnaK (Caplan et al., 1993).

We have started to isolate different domains of DnaJ for structural and biochemical characterization. For this initial report, we targeted the J-homology region of DnaJ, DnaJ(1−78). On the basis of the sequence homology arguments cited above this domain would appear to be the minimum length required for interaction with DnaK or Hsp70 homologs, yet this domain has not demonstrated the ATPase stimulatory activity of a DnaJ(1−104) (Szabo et al., 1994). However, since the C-terminal extension appears missing in related systems such as the budding yeast protein Sec63, which still interact with DnaK homologs (Silver & Way, 1993), we decided to focus on this minimal structural element before considering an extension that promotes specific enzyme activity. We have successfully cloned, overexpressed, and purified DnaJ(1−78) and have obtained a well-behaved, uniformly ^{15}N-labeled sample for structure determination by standard 2D and 3D NMR techniques. Here we present our assignment strategy along with the ^{1}H and ^{15}N chemical shift assignments and a discussion of a preliminary structure of this fragment.

MATERIALS AND METHODS

Cloning and Overexpression of DnaJ(1−78). The expression of the J-homology domain of *E. coli* DnaJ was directed from the plasmid pDnaJ(1−78)11d in *E. coli* strain MgT7 (gift of Dr. D. LeMaster). The expression plasmid pDnaJ(1−78)11d was constructed by ligating PCR-amplified DNA encoding the first 78 residues of DnaJ into the plasmid pET11d that contains the strong bacteriophage T7 promoter (Studier et al., 1990). The amplification was directed from two primers: one (5′-GCAATTTAAAACCATGGCTAAGCAAGAT), which introduces an *Nco*I restriction site into codons −1,1, and the other (5′-CAAAACCGCCGGATCCTTAGCCTTGCTC), which introduces a TAA stop codon into codon 79 followed by a *Bam*HI restriction site. The PCR-amplified DNA fragment was restricted with *Nco*I and *Bam*HI and then ligated into the complementary sites in pET11d.

Growth of MgT7-pDnaJ(1−78)11d and expression of unlabeled DnaJ(1−78) was accomplished in TB media at 37 °C as described below. ^{15}N-Labeled DnaJ(1−78) was overexpressed in *E. coli* grown in MOPS minimal media containing $^{15}NH_4Cl$ (99% enrichment) as the sole nitrogen source (Neidhardt et al., 1974). For growths to produce ^{15}N-DnaJ(1−78), the cells were grown at 37 °C to an OD_{600} of 1.0, and then protein production was induced by addition of IPTG to a final concentration of 0.4 mM. The cultures were grown an additional 3 h (OD_{600} ~2.5) after which time the cells were harvested by low-speed centrifugation. Cell pellets were frozen and stored at −80 °C until used.

Frozen, induced *E. coli* [MgT7-pDnaJ(1−78)11d] paste was thawed by suspension in $^{1}/_{20}$th of the original culture volume of 100 mM Tris-HCl, pH 8.0, 0.1 mM EDTA, and 1 mM PMSF (added just prior to use). DNase I was added to the cell suspension to a final concentration of 0.01 mg/mL, and cell lysis was promoted, on ice, by probe sonication using a 10-mm tip, at the highest power setting, for three cycles of 1 min on and 1 min off. The crude lysate was incubated for 20 min, on ice, to allow for hydrolysis of DNA. Cellular debris was removed by centrifugation at 40 000 rpm in a Beckman 45Ti rotor for 60 min. The supernatant was adjusted to 50 mM NaCl by addition from a 5 M stock solution, and the pH was lowered to 7.2 by addition of solid MOPS. The cleared supernatant was loaded onto a DEAE cellulose column (~1.0-mL bed volume/mL of extract) that had previously been equilibrated with 50 mM Tris-HCl, pH 7.5, 0.1 mM EDTA, 50 mM NaCl (TREN buffer). Under these conditions, DnaJ(1−78) does not bind tightly to the column. The flow through and first 1.5 column volumes of a wash with TREN buffer were pooled, and the pH was adjusted to 6.8 with solid MOPS. The pooled pH-adjusted DEAE eluent was then applied to a 50-mL SP-cation-exchange column [Fractogel EMD SP-650(M), EM Science] equilibrated with 25 mM MOPS, pH 6.8, and 0.1 mM EDTA (SP buffer). The column was washed with 100 mL of SP buffer, and the protein was then eluted during a 500-mL linear gradient from 0 to 500 mM NaCl in SP buffer. DnaJ(1−78) eluted as the major 280-nm absorbing peak from this column. Fractions corresponding to the highest purity material as judged by SDS−PAGE were pooled and concentrated to approximately 20 mg/mL by ultrafiltration using a YM3 membrane. The concentrated DnaJ(1−78) was further purified, in 2-mL aliquots, by size-exclusion chromatography on a 600 × 21.5 mm TSK-250 column (Bio-Rad) equilibrated with 25 mM MOPS, pH 6.8, and 100 mM KCl. Fractions containing DnaJ(1−78) were pooled and dialyzed against 10 mM Tris-HCl, pH 7.5, and 50 mM KCl and then loaded onto a 35-mL hydroxyapatite column equilibrated with 10 mM PO_4, pH 6.8, and 50 mM KCl (HAP buffer). The HAP column was washed with 50 mL of HAP buffer, and the protein was then eluted in a 300-mL linear gradient from 10 to 400 mM PO_4 plus 50 mM KCl. Peak fractions were concentrated to approximately 40 mg/mL by ultrafiltration with a 3 kDa nominal molecular mass cutoff membrane and dialyzed exhaustively against 10 mM Tris-HCl, pH 7.5, 100 mM KCl, and 0.1 mM EDTA. The purified, dialyzed protein was frozen and then stored at −80 °C until used. DnaJ(1−78) concentration was determined either by quantitative amino acid analysis or using an extinction coefficient at 280 nm of 10 000 L mol^{-1} cm^{-1}. The yields of pure protein were around 140 mg/L of SB media and 40 mg/L of minimal media.

CD Spectroscopy. Circular dichroism spectroscopy was performed on an AVIV Model 60DS spectrophotometer (Lakewood, NJ) or at the National Synchrotron Light Source (NSLS) using a vacuum UV spectrometer mounted on the U9 beam line (Sutherland et al., 1980, 1982). All CD spectra were collected on a 0.1 mM sample of DnaJ(1−78) in 1 mM PO_4, pH 6.0. For spectra collected at the NSLS, a 0.010-mm Gray cell (Gray et al., 1984) was used, and a scan from 260 to 174 nm was run at 25 °C with data collected every 0.5 nm. The temperature study from 30 to 95 °C and back to 30 °C was monitored at 222 nm; data were collected every 1.0 °C with a 3.0-min equilibration time and a 30-s acquisition at each data point.

NMR Spectroscopy. All NMR experiments were performed at 30 °C on a General Electric Ω500 spectrometer operating at 500.066 MHz and equipped with an S-17 gradient accessory. Heteronuclear spectra were collected on 4 mM uniformly ^{15}N-labeled DnaJ(1−78) and 50 mM PO_4, pH 6.0, in 90% H_2O/10% D_2O. Homonuclear spectra were obtained on a 2 mM unlabeled sample under similar buffer conditions. ^{1}H chemical shifts are referenced to TSP at 0.0

ppm, and ^{15}N chemical shifts are reported relative to liquid ammonia at 0.0 ppm (Live et al., 1984).

2D Homonuclear Experiments. A clean HOHAHA spectrum was acquired using a 60-ms MLEV-17 spin lock with a homospoil z-filter at the end of the mixing time (Bax & Davis, 1985; Griesinger et al., 1988). NOESY spectra were obtained by standard methods at mixing times of 100 and 200 ms. The 100-ms set used for structural analysis was collected on the 2 mM unlabeled sample. A DQF-COSY spectrum was also collected to measure the $^3J_{HNH\alpha}$ coupling constants by the method of Kim and Prestegard (1989). In all these homonuclear experiments, presaturation of the water signal was achieved by DANTE selective irradiation (Morris & Freeman, 1978). Acquisition times, 78.2 ms in t_1 for 416 complex points and 186 ms in t_2 for 1024 complex points, were also the same for each homonuclear run.

$^1H-^{15}N$ Heteronuclear Experiments. For all heteronuclear experiments, the ^{15}N carrier was placed in the middle of the amide region at $\delta = 114.0$ ppm. Either a 2D $^1H-^{15}N$ GSE-HSQC (Kay et al., 1992) or 2D $^1H-^{15}N$ GE-HMQC (Tolman et al., 1992) was collected before and after each 3D heteronuclear experiment to validate the integrity of the sample. In these routine experiments, which were collected in under 3 min, the number of t_1 complex points was 32 with a 26.2-ms acquisition time, and the number of complex points in t_2 was 512 with a 92.9-ms acquisition time. A higher resolution $^1H-^{15}N$ GSE-HSQC was obtained with a t_1 acquisition time of 384 ms (512 complex points) and a t_2 acquisition time of 92.9 ms (512 complex points). To characterize backbone amide protons that exchange slowly with the solvent, the ^{15}N-labeled protein was lyophilized and redissolved in D_2O, and ^1H-^{15}N GSE-HSQC spectra (60.8 ms in t_1, 92.9 ms in t_2) were acquired every 5 min for the first 2 h, every 10 min for the next 12 h, and then once every 24 h for 6 days. The exchange rates were quantitated as described previously (Andrec et al., 1995).

A 3D $^1H-^{15}N$ HOHAHA-HMQC spectrum was acquired using a sequence based on that previously published (Marion et al., 1989a). The water signal was presaturated off-resonance using a Shinnar−Leroux selective irradiation (Leroux, 1988; Shinnar et al., 1989). The ^1H carrier was placed at 5.9 ppm for good Hartmann−Hahn mixing, and the coherence transfer was accomplished using a DIPSI-2 mixing scheme for 60 ms (Shaka et al., 1988) followed by a 30-ms NOE delay to offset the positive ROE during isotropic mixing (Marion et al., 1989a). The spectral parameters were a t_1 acquisition time of 23.3 ms for the indirect ^1H dimension (128 complex points), t_2 acquisition time of 26.2 ms for the ^{15}N dimension (32 complex points), and a t_3 acquisition time of 146 ms for the directly observed ^1H dimension (512 complex points). Eight scans per point were collected with a recycling rate of 0.83 s^{-1}. The F_2 indirectly detected proton dimension was unfolded during processing as described by Kay et al. (1989).

The 3D $^1H-^{15}N$ GE-NOESY-HMQC was similar to that of Kay et al. (1989; Marion et al., 1989b) with the exception of the HMQC detection, in which the gradient-enhanced HMQC of Tolman et al. (1992) was incorporated. The ^1H carrier was placed in the middle of the amides at 7.83 ppm, and no presaturation of water was necessary. A NOESY mixing time of 200 ms was collected with the same acquisition parameters as the above 3D $^1H-^{15}N$ HOHAHA-HMQC except for the directly detected proton dimension in which the acquisition time was 165 ms for 512 complex points. Four transients per point were collected with a recycling rate of 1.18 s^{-1}.

A 3D $^{15}N-^1H-^{15}N$ GE-HSQC-NOESY-HSQC developed here by K. R. MacKenzie (unpublished experiments) was collected at mixing times of 100 and 200 ms with no presaturation. This experiment is a derivative of a four-dimensional experiment introduced by Vuister et al. (1993a), which allows the observation of NOE connectivities between peaks in a pair of two-dimensional HMQC experiments (HMQC-NOESY-HMQC). In our case the HSQC experiment, which generally provides higher resolution and sensitivity for macromolecular systems, has been substituted for the HMQC segments, and the gradient-selected, enhanced-sensitivity version of the HSQC experiment introduced by Kay et al. (1992) has been used for the last HSQC segment. The proton evolution period in the first HSQC segment has also been reduced to a fixed period of pure scalar coupling (J) evolution of length $1/2J$. This produces a three-dimensional ^{15}N, ^{15}N, ^1H experiment that can be acquired with limited amounts of spectrometer time. Both F_1, F_2 indirectly detected ^{15}N dimension acquisition times (t_1 and t_2, respectively) were 48 ms for 64 complex points, and the F_3 directly observed proton dimension acquisition time, t_3, was 85.2 ms for 512 complex points. Four scans per point were collected with a recycling rate of 0.77 s^{-1}.

A 3D $^{15}N-^1H$ HNHA experiment (Vuister & Bax, 1993b) was collected to verify and supplement the coupling constant data from the homonuclear DQF-COSY spectrum. The spectral parameters were a t_1 acquisition time of 52 ms for the constant time ^{15}N dimension (64 complex points), a t_2 acquisition time of 3.4 ms for the ^1H dimension (17 complex points), and a t_3 acquisition time of 146 ms for the directly observed ^1H dimension (512 complex points). Thirty-two scans were collected for each pair of t_1/t_2 points at a repetition rate of 1.0 s^{-1}.

Quadrature detection in all indirectly detected dimensions was obtained by using either States, States−TPPI, or gradient methods (Marion et al., 1989b; Marion & Wüthrich, 1983; States et al., 1982; Tolman et al., 1992). Spectra were processed using FELIX 2.1 (Biosym, Inc.). Data Analysis was accomplished using a combination of FELIX routines and the relational database (DBASE IV, Borland, Inc.) routines developed in-house.

Molecular Modeling. The program X-PLOR (Brünger, 1992) was used to generate structural models for DnaJ(1−78) using NMR-derived distance and torsion angle constraints. Distance constraints extracted from NOE data were applied to midpoints between pairs of nuclei in cases where stereospecific assignment was not possible. In these cases, distances were corrected on the basis of known amino acid geometries. The constraints were represented in the form of an asymmetric internuclear pseudoenergy having a minimum at the constraint distance, a harmonic wall to the short-distance side of a lower bound, and a harmonic function making a transition to a zero slope asymptote to the long-distance side of an upper bound. The bounds were offset from the constraint distance 6% of the square of the distance constraints for proton−proton pairs (0.7 Å for a 3.5-Å constraint) and were expanded by 0.8−1.5 Å in cases where average proton positions were used. A weighting factor of 25 was used to scale these constraint energies. The search protocol involved a distance geometry phase followed by

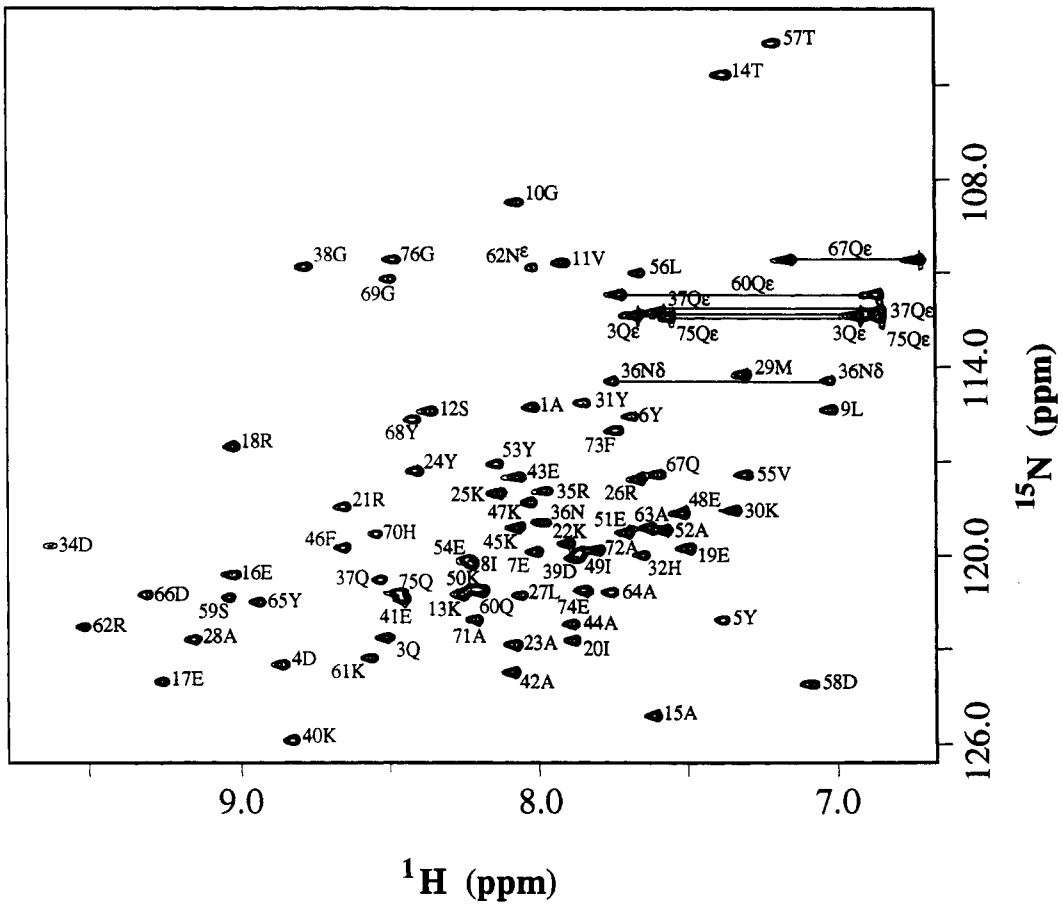

FIGURE 1: $^{1}H-^{15}N$ GSE-HSQC spectrum of ^{15}N-labeled DnaJ(1−78). One peak is observed for every backbone amide proton as labeled. The side-chain NH_2's of the five glutamines and asparagine-36 are indicated by solid lines connecting their two proton resonances at the ^{15}N chemical shift of the shared nitrogen. Complete chemical shift assignments are given in Table 1 of the supplementary material. All spectral data presented in this paper were collected at pH 6.0, 30 °C, and at 500.066-MHz proton frequency.

three cycles of simulated annealing in which the temperature was brought to 2000 K and slowly cooled. These calculations were run on an IndyR4400 workstation (Silicon Graphics Inc.) and typically required 20 min per structure for generation.

RESULTS

General Solution Properties of DnaJ. Before undertaking a detailed NMR investigation of secondary structure, it is useful to confirm the presence of a well-defined structural domain under the conditions of our experiments and to know something of the general composition of secondary structural elements. The CD spectrum provides much of this information. The spectrum of a 0.1 mM sample in 1 mM PO_4, pH 6, is typical of that observed for proteins that are predominately α-helical, as evidenced by large negative bands of ellipticity at 208 and 222 nm and a large positive band at 190 nm (Johnson, 1990). Quantitative analysis of this CD spectrum, using the algorithm of Hennessey and Johnson (1981), indicates the absence of any substantial amount of β-sheet and suggests that approximately 70% of the residues adopt an α-helical conformation, 15% are in a turn conformation, and 15% are in other nonstandard conformations. To investigate the stability of this fragment, we examined the temperature dependence of the ellipticity at 222 nm. The thermal unfolding curve of DnaJ(1−78) shows a substantial, and reversible, transition with a T_m of 75.1 °C. The van't Hoff enthalpy, ΔH_{vH}, for the transition was determined from the slope of a plot of ln K_{app} vs $1/T$ ($R = 0.998$). For DnaJ-(1−78), the ΔH_{vH} is 65.1 kcal/mol. Comparison to preliminary calorimetric data obtained at 3 mM suggests that while there is a small tendency toward aggregation, the protein fragment under conditions of our experiments would be predominately monomeric. The CD data, thus, suggest stability and well-defined secondary structure for a monomeric domain that can in principle be characterized in more detail using NMR methodologies.

Assignment of NMR Spectra. Figure 1 shows the data from a $^{1}H-^{15}N$ GSE-HSQC where one cross-peak is observed for every main-chain amide proton. This indicates the fragment is in a single conformation on the NMR time scale. The dispersion in the ^{15}N dimension combined with that in the ^{1}H dimension is sufficient to unambiguously resolve nearly all resonances. The side-chain NH_2 resonances from asparagine-36 and the five glutamines are also present as labeled.

The assignment of cross-peaks is based on a traditional combination of through-bond correlation experiments to assign amino acid types and through-space correlation experiments to make sequential connectivities. The assignment was facilitated using a relational database (DBASE IV) to expedite the process. First, cross-peaks in a 3D $^{1}H-^{15}N$ HOHAHA-HMQC spectrum showing connectivities within a scalar-coupled spin system were picked using the automatic routines present in FELIX 2.1, and the list was edited in an interactive display mode. A text file of peak position and

volume was then converted to a relational database. A DBASE program sorted the data and assigned all peaks at the same amide proton chemical shift and the same amide nitrogen chemical shift to one spin system. The systems were given a default amino acid type and an arbitrary residue number. Automatic presentation of sets of peaks belonging to a single spin system allowed assignment to a particular class of amino acid and in many cases a unique amino acid type. Second, these initial assignments were transferred to a 3D $^1H-^{15}N$ NOESY-HMQC database containing both intra- and interresidue, through-space connectivities. Intraresidue assignments were made using a DBASE program that sought the best match for expected intraresidue amide−α and amide−β cross-peaks. All remaining peaks on an amide proton−amide nitrogen column were assumed to be interresidue and simply labeled as to their amino acid of origin.

Automatic assignment of interresidue cross-peaks was initially based on a search for the best chemical shift match with an assigned intraresidue peak. In many cases, interresidue peaks in the NH−Cα region were assigned unambiguously but where this was not possible the program kept a list of alternatives for manual examination. Comparison of amino acid spin systems, now connected by traditional $d_{\alpha N}(i, i+1)$ correlations, with the known DnaJ(1−78) sequence allowed proper identification of residue numbers in about 30% of the cases. With these few segments automatically assigned, manual identification of additional amino acid types and placement in sequential positions became possible. Once the amino acids were assigned to sequential positions, remaining unassigned cross-peaks with high levels of ambiguity were assigned, giving preference to assignments which corresponded to short-range sequential connectivities.

The majority of the assignments were made in the above manner and verified manually. As expected, $d_{\alpha N}(i, i+1)$ correlations are seen for nearly all the residues, and where they are missing, the $d_{\beta N}(i, i+1)$ connectivities support the sequential assignment. In some cases, it was necessary to manually examine data from the homonuclear 2D HOHAHA and homonuclear 2D NOESY, where the digital resolution was much better (6.6 Hz/point), to resolve ambiguities. Except for P33 and one residue near the amino terminus, all backbone ^{15}N and ^1H peaks could be assigned using the ^{15}N correlated data. Assignment of many of the side-chain ^1H resonances was also possible; however, the mixing time and signal to noise ratio of the 3D $^1H-^{15}N$ HOHAHA-HMQC prohibit the identification of resonances beyond the β-protons in several amino acid side chains. Side chain assignments were therefore extended using homonuclear 2D spectra. The proton and nitrogen chemical shift assignments are presented in Table 1 of the supplementary material.

Secondary Structure Indications. For a predominantly α-helical protein one would expect to see relatively weak $d_{\alpha N}(i, i+1)$ connectivities, strong $d_{NN}(i, i\pm1)$ connectivities, and weak but highly useful $d_{\alpha N}(i, i+3)$ and $d_{\alpha N}(i, i+4)$ connectivities (Wüthrich, 1986). In DnaJ(1−78), most residues in the segments 5−10, 17−30, 51−56, and 59−69 showed this pattern for $d_{\alpha N}(i, i+1)$, $d_{NN}(i, i\pm1)$, and $d_{\alpha N}(i, i+3)$ cross-peaks. Weak $d_{\alpha N}(i, i+4)$ connections were also observed between E7 and V11, E17 and R21, K25 and M29, A52 and L56, S59 and A63, and Y65 and G69, confirming the presence of an α-helix in these regions. Plots showing NH−Cα NOE and NH−NH correlations for residues S59 through G69 are included in the supplemental figures as an example of the connectivities observed. A table of assigned NOE connectivities is also included.

Unfortunately, the NH−Cα segment containing residues E41−I49 was difficult to classify. There appears to be some $d_{\alpha N}(i, i+3)$ connections, but due to spectral overlap in the indirectly detected proton (F_1) dimension in the 3D $^1H-^{15}N$ GE-NOESY-HMQC, assignment of these connectivities was often ambiguous. The NH−NH region also shows extensive resonance overlap. The homonuclear 2D NOESY afforded enough resolution to remove some of these ambiguities and suggests this stretch of amino acids may also adopt an α-helical conformation.

An illustration of the difficulties encountered with the E41−I49 segment is shown in Figure 2a. This figure shows ^{15}N slices from the 3D $^1H-^{15}N$ GE-NOESY-HMQC. Here, the $d_{NN}(i, i+1)$ correlation and the expected $d_{NN}(i, i-1)$ reverse correlation are seen for many adjacent amino acids. For example, the forward and reverse connections between E41 and A42 are clear. However, it is impossible to determine whether a connection between A42 and E43 exists. This particular ambiguity arises because the amide proton frequency is the same for A42 and E43. Also, both E43 and K45, which are degenerate in amide proton frequency, show a correlation to A44; however, because of overlap, it cannot be determined whether only one or both of the expected correlations from A44 to E43 and to K45 exist. Similarly, both K45 and K47 are degenerate in amide proton chemical shift and show correlations to F46, yet, once again, whether F46 shows a correlation to K45, to K47, or to both is unclear due to spectral overlap.

The difficulties mentioned above can potentially be circumvented using a 3D $^{15}N-^1H-^{15}N$ GE-HSQC-NOESY-HSQC experiment. This experiment labels amide proton magnetization with the chemical shift of its directly bonded ^{15}N before it is used as a source of magnetization for NOE transfers. Since ^{15}N chemical shifts are not nearly so degenerate as ^1H, they can often provide the necessary resolution for the evaluation of connectivities. Columns from the point in the F_2, F_3 plane corresponding to an intraresidue amide nitrogen−amide proton pair now contain NOE cross-peaks at the ^{15}N chemical shift, as opposed to the ^1H chemical shift, of an interresidue partner. Provided that the ^{15}N frequencies of the two residues involved in the correlation are not degenerate, the NOE is easily identified. In Figure 2b are ^{15}N slices from the 3D GE-HSQC-NOESY-HSQC data for the same region presented in Figure 2a. Now it is possible to determine the presence of a correlation between A42 and E43. Also, we now clearly observe that A44 shows a cross-peak to both E43 and K45. Likewise, F46 shows correlations to both K45 and K47. With the aid of these correlations, we confirmed the presence of an α-helix between A42 and I49. Figure 3 summarizes the observed NOE contacts useful in characterizing secondary structure.

To further support identification of helical segments, the $^3J_{HNH\alpha}$ coupling constants were determined from a homonuclear DQF-COSY and an ^{15}N-edited HNHA experiment. For the homonuclear experiment, the data were analyzed as described by Kim and Prestegard (1989), and for the heteronuclear experiment, the data were analyzed as described by Vuister and Bax (1993b). Coupling constant values under 7 Hz were taken to be indicative of α-helices, whereas larger values indicate β-sheet or extended structure (Wüthrich, 1986). The data are summarized in Figure 3 and

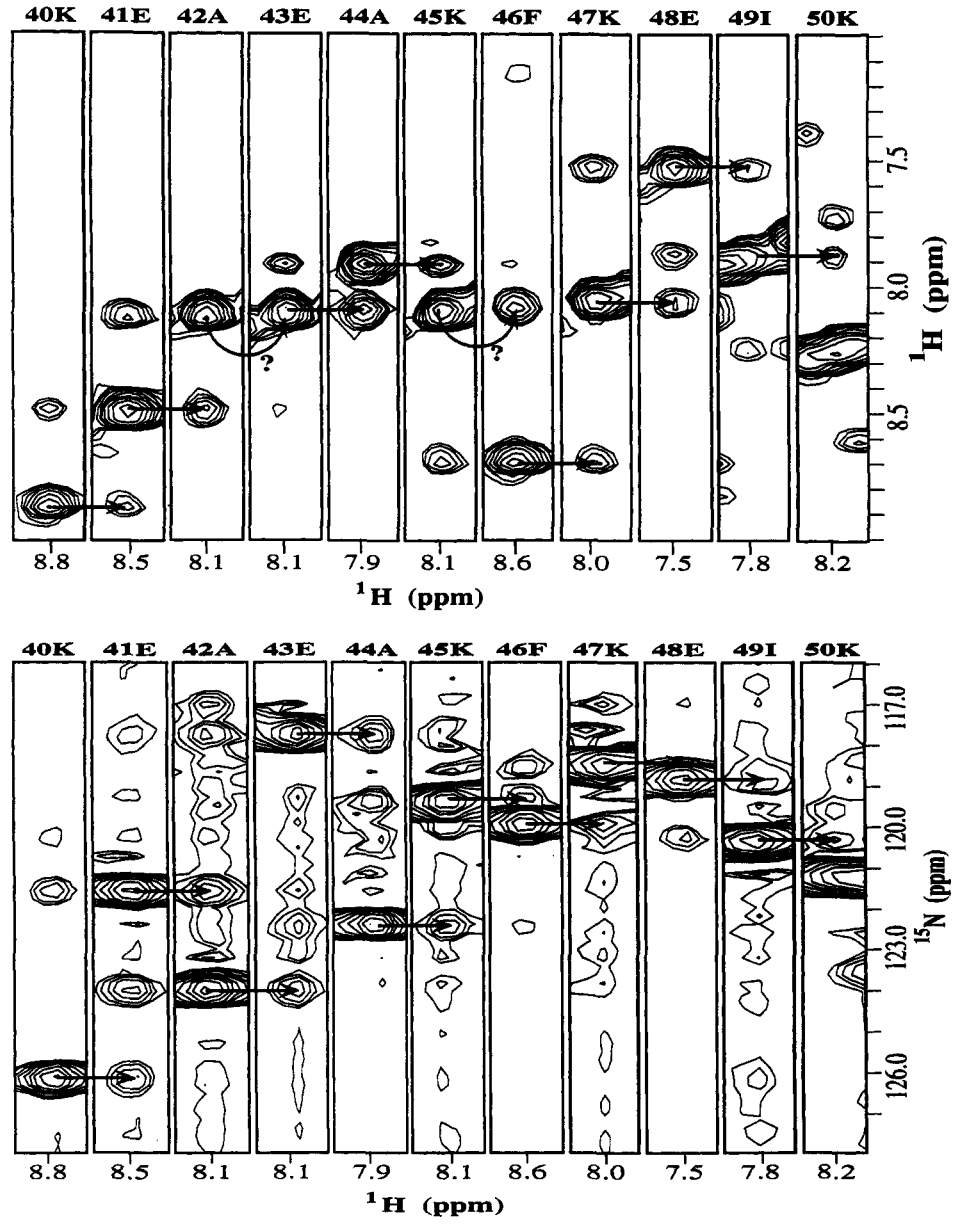

FIGURE 2: Amide−amide NOE data for residues K40 through K50 from two different, but related, experiments. In (a, top), sequential ^{15}N slices from the 200-ms, 3D ^{1}H−^{15}N GE-NOESY-HMQC data set are shown. Each slice is at the ^{15}N chemical shift of the amide nitrogen of the residue indicated at the top of the slice. Straight arrows indicate $d_{NN}(i, i+1)$ NOE connectivities typically observed in α-helices. The curved arrows point to areas of ambiguity due to lack of spectral resolution. These ambiguities are resolved by the 100-ms, 3D ^{15}N−^{15}N−^{1}H GE-HSQC-NOESY-HSQC, as seen in (b, bottom), and allow this region to be clearly classified as adopting an α-helical conformation. See text for further discussion.

are consistent with NOE data indicating the presence of four α-helices: I (D4−G10), II (E17−K30), III (A42−L56), and IV (K61−G69).

Reverse turns in proteins can also give rise to distinctive NOE and scalar coupling patterns. Among the most distinguishing characteristic is the presence of moderate $d_{\alpha N}(i, i+2)$ NOEs between the second and fourth element of a four-residue turn and the presence of $d_{NN}(i, i+1)$ NOEs between the third and fourth elements that are stronger than those normally present in α-helices (Wüthrich, 1986). NOE connectivities among residues S12−A15 between helix I and helix II fit this pattern. The presence of a weak $d_{\alpha N}(i, i+3)$ NOE between residues S12 and A15 and the presence of a moderate $d_{NN}(i, i+1)$ NOE between residues K13 and T14 suggest that this is a type I rather than type II turn. The fact that $^3J_{HNH\alpha}$ for K13 is less than 3 Hz and for T14 is about 10 Hz is also more consistent with a type I than type II turn.

There are several other cases where the presence of $d_{\alpha N}(i, i+2)$ NOEs suggest turns, but in most cases, their existence cannot be confirmed through the observation of other expected NOE and coupling constant patterns. A possible exception is the segment from Y31 to D34 at the end of helix II. A moderate $d_{\alpha N}(i, i+2)$ NOE is observed between H32 and D34. The confirming strong $d_{NN}(i, i+1)$ NOE between the third and fourth elements is not expected in this case because residue 33 is a proline. The $^3J_{HNH\alpha}$ value for H32 is small as expected for a reverse turn. This, coupled with the relatively high tendency of proline to occur in turns (Richardson, 1981), leads us to identify a turn after helix II.

Hydrogen−deuterium exchange experiments were used to investigate the stability of elements of secondary structure.

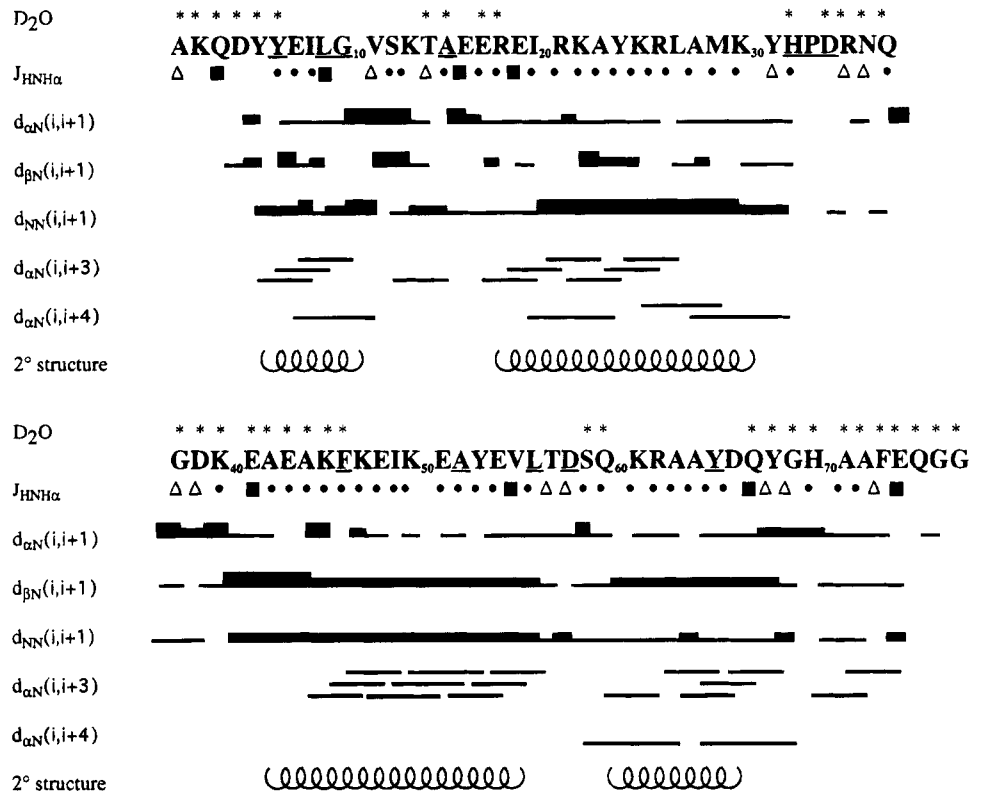

FIGURE 3: Summary of NMR data for DnaJ(1−78), pH 6.0, 30 °C. The underlined residues indicate the most highly conserved residues of the J-homology domain. The asterisks in the row above the amino acid sequence depict which amide protons exchange quickly after dissolution in deuterated buffer. The row below the amino acid sequence summarizes the $^3J_{HNH\alpha}$ data: filled circles, $J < 6$ Hz; open triangle, $J > 8$ Hz; and filled squares, $J = 6-8$ Hz. The bars below the sequence represent the observed NOE connectivities: $d_{\alpha N}(i, i+1)$, $d_{\beta N}(i, i+1)$, $d_{NN}(i, i+1)$, $d_{\alpha N}(i, i+3)$, and $d_{\alpha N}(i, i+4)$. The thickness of the bar depicts the intensity of the NOE. Regular secondary structure is indicated at the bottom.

We collected a series of 2D $^1H-^{15}N$ GSE-HSQC experiments, immediately following the dissolution in D_2O of the protonated DnaJ(1−78), which allowed measurement of the exchange rate of backbone amide protons. Quickly exchanging amide protons are typical of a lack of well-defined secondary structure or exposure to solvent while more slowly exchanging amides are more likely involved in some form of stable secondary structure or are well protected from solvent (Englander & Kallenbach, 1984; Englander & Mayne, 1992). The exchange rates that were measurable are reported in Table 1, and the more rapidly exchanging amides are identified by asterisks in Figure 3. The backbone amides involved in both helix I and helix II are slow to exchange, which confirms the presence of these α-helices and suggests a high level of stability. The exchange data from helix III is not as straightforward to interpret. The amide protons of the first half of the helix from A42 to F46 are completely exchanged away within the first 10 min after D_2O dissolution. Yet, the amide protons of the latter half of helix III from residues E50 to S59 are quite long lived. The amide protons from helix IV are almost as short-lived as those from the first half of helix III, having all exchanged away within the first 30 min after D_2O dissolution. Thus, helices I and II are quite stable. While helices III and IV are present, there is clearly a lower level of stability with respect to amide exchange.

General Fold of DnaJ(1−78). The overall fold of a protein is determined by long-range (>5 residues apart) distance constraints generated from the NOE experiments. These NOEs indicate which segments of the protein are in close contact with other segments that may be far away in primary sequence. Typically, these long-range NOEs are found between side-chain protons and not between backbone protons. The ^{15}N-based $^1H-^{15}N$ GSE-NOESY-HMQC experiment is not the best source of these connectivities because most NOE transfers detected are to amide backbone protons. Homonuclear 2D NOESY spectra provide a better option, but many assignments are ambiguous because of spectral overlap. We have, however, been able to extract NOEs involving relatively well resolved pairs of resonances from a 2D NOESY spectrum with a 100-ms mixing time and use these NOEs to generate a preliminary three-dimensional structure. Ultimately these preliminary structures can be used

Table 1: Backbone Amide Exchange Rates Observed in DnaJ(1−78), pH 6.0, 30 °C[a,b]

helix I		helix II		helix III		helix IV	
res	k_{ex}	res	k_{ex}	res	k_{ex}	res	k_{ex}
Y6	2.31	I20	2.53	K47	~102	K61	19.4
E7	4.95	R21	6.49	E48	~105	R62	~77
I8	2.38	K22	12.5	I49	15.0	A63	~105
L9	1.26	A23	4.84	K50	3.42	A64	~105
G10	5.08	Y24	2.96	E51	4.80	Y65	~134
		K25	14.1	A52	2.54	D66	~134
V11	1.96	R26	31.0	Y53	1.77		
A15	23.4	L27	8.33	E54	2.17		
		A28	21.1	V55	1.30		
				L56	1.75		
				T57	4.90		
				D58	16.5		

[a] Rates are expressed in $min^{-1} \times 10^{-3}$; those rates greater than 0.075 min^{-1} are based on only one intensity measurement and therefore are only a rough estimate of the lower limit. [b] Residues not listed have rates greater than 0.134 min^{-1}.

Table 2: Long-Range NOE Connectivities Observed in 2D $^1H-^1H$ NOESY of DnaJ(1−78), pH 6.0, 30 °C[a]

residue, proton	residue, proton	residue, proton	residue, proton
Y5, he*	A52, hb*	L9, hd*	L56, hd*
Y5, he*	V55, hg*	Y24, he*	F46, he*
Y5, he*	V55, hg*	Y24, hd*	I49, hg2*
Y5, hd*	V55, hg*	Y24, he*	I49, hg2*
Y6, he*	L56, hd*	Y24, he*	K50, ha
Y6, he*	L56, hd*	V55, hg*	R62, hb*
L9, hd*	L56, hg	V55, hg*	Y65, hd*
L9, hd*	I49, ha	V55, hg*	F73, hd*
L9, hd*	Y53, hd*	V55, hg*	F73, he*
L9, hd*	Y53, he*	L56, ha	R62, hg*
L9, hd*	L56, hd*	L56, hb*	R62, hb*
L9, hd*	L56, hd*	L56, hg	R62, hg*

[a] An asterisk indicates that stereospecific assignments have not been made.

to resolve ambiguity in the 2D data set and provide higher resolution structures. Twenty-four long-range constraints used to generate structures are listed in Table 2. The list is dominated by contacts involving hydrophobic residues that appear to be a part of a hydrophobic core involving the beginning of helix I, the middle of helix II, the end of helix III, the middle of helix IV, and a single phenylalanine found near the C-terminus. Contacts involving helices I and III, II and III, and IV and III are all represented. This suggests a well-formed, folded structure. The NOEs represented in Table 2 were converted to distance constraints using an initial rate approximation and assumed $1/r^6$ dependence for cross-peak volumes. Secondary structure elements as depicted in Figure 3 were constrained using typical α-helical backbone torsional angle constraints and i to $i+4$ hydrogen-bonding constraints between carbonyl oxygens and amide protons.

The long-range and secondary structure constraints were used in the program X-PLOR (Brünger, 1992) to generate tertiary folds that are consistent with the NMR data. Twenty structures were generated, among which 14 showed no violations of distance constraints within 0.5 Å of the constraint bounds. One of the lowest energy structures is shown in Figure 4. All zero violation structures, including this one, show antiparallel packing of helices II and III with an exposed loop between residues 31 and 40. The exact positions of helices I and IV differ in the various structures but in all cases fold against the central helices and remain near the region encompassing the N-terminus of helix II and C-terminus of helix III as depicted in Figure 4. The loop containing some of the most conserved residues in DnaJ, Y31−D34, is well exposed at the opposite end of this antiparallel pair.

DISCUSSION

Given the DnaJ homology data along with the precedence for a modular architecture of proteins (Bork, 1992; Bork et al., 1992; Patthy, 1991), and the recent examples of functional and structured protein domains (Booker et al., 1992; Overduin et al., 1992; Waksman et al., 1993), it is not unreasonable to expect the independent 1−78 fragment of DnaJ to be biochemically and structurally well-behaved. This expectation is easily confirmed from the results presented above. The domain contains a high percentage of recognizable secondary structure based on the CD spectrum alone. The temperature dependence of the CD

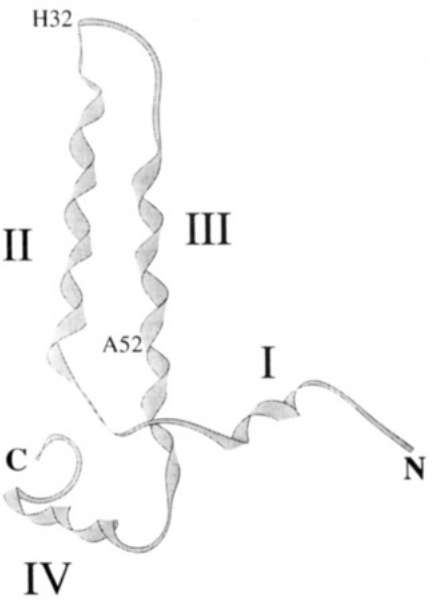

FIGURE 4: Layout of the four α-helices found in DnaJ(1−78). Two of the key functional residues discussed in the text are indicated. This figure was generated by MIDAS.

spectrum also indicates a high level of stability. The melting transition is sharp and the van't Hoff enthalpy is high. From the value of ΔH_{vH} and the measured T_m, the free energy of stabilization, ΔG, at 25 °C is calculated to be 12−14 kcal/mol. The values of ΔH_{vH} and ΔG at 25 °C have both been confirmed by differential scanning calorimetry and indicate that the J-homology domain of DnaJ is remarkably stable.

DnaJ(1−78) as a stable, folded domain is also supported by hydrogen−deuterium exchange experiments, which are classically used as an evaluation of a protein's structural stability. It is widely documented that a well-structured protein's amide protons, involved in secondary structure or in other ways shielded from solvent, will persist for periods of days or more after dissolution in deuterated buffer (Englander & Kallenbach, 1984; Englander & Mayne, 1992). The DnaJ(1−78) exchange data confirm the presence and stability of two well-formed helices: helix I (D4−G10) and helix II (E17−K30). The last half of helix III (E50−L56) is also stable with the amide proton of V55 still persisting 6 days after dissolution in D_2O. Low stability of otherwise recognizable secondary structural elements (the first half of helix III and all of helix IV) is not unprecedented in the literature (Andrec et al., 1995). However, it is also, in principle, possible that the C-terminal element is unstable because of the absence of interactions with subsequent elements that would be present in the full-length native structure.

While the number of long-range NOE constraints reported here is inadequate for a high-resolution three-dimensional structure, they do provide some evidence for the positioning of helix IV as shown in Figure 4. Helix IV is positioned as depicted largely by contacts between helix III and just two residues, R62 and Y65, of helix IV. One could argue that these are the result of transient contacts that would be more long lived if additional parts of the native structure were included. With respect to the positioning of helix IV, it is of interest to note that while this work was under review, a structure for a somewhat larger domain of DnaJ, DnaJ(1−107), appeared in the literature (Szyperski et al., 1994). Placement of secondary structural elements in the larger

domain is identical to that described here within ±2 residues, and the tertiary fold for helices I, II, and III is similar. However, the extension of the C-terminal end is reported as disordered for the larger domain, and the only residue in helix IV showing long-range NOE contacts to the remainder of the structure is reported to be Y65. Thus, while helix IV may not be well positioned in DnaJ(1−78), modest elongation of the sequence does not seem to restore association of helix IV with the remainder of the domain. If anything, these interactions are enhanced in DnaJ(1−78) over that seen in the larger domain studied by Szyperski et al. (1994).

It is useful to review previous biochemical and holistic data on DnaJ. Earlier secondary structure prediction algorithms suggested that the J-homology domain contained two α-helices separated by a turn at H32−P33−D34 (Silver & Way, 1993; Wall et al., 1994), the three residues which are absolutely conserved across the known J-homology domains (Bork et al., 1992; Silver & Way, 1993). The data presented here are consistent with the postulated turn at Y31−D34. This turn separates helix II from a short loop, R35−E41, in our structural model. It is also possible to use the structural model presented in Figure 4 to help in interpreting previous mutational studies. Single point mutants in the J-homology region which alter normal function have been characterized in *E. coli* and budding yeast, *Saccharomyces cerevisiae*. Georgopoulos and co-workers recently characterized such a mutant of DnaJ, H32Q (Wall et al., 1994). This mutant does not interact with DnaK on the basis of its failure to either stimulate DnaK's ATPase activity or significantly change DnaK's conformation in the presence of ATP. Similar mutants in the J-homology domain of Sec63, the budding yeast Hsp40, have been examined by Feldheim et al. (1992), in which the investigators used site-specific mutagenesis to change the invariant P157N and D158A, which correspond to P33N and D34A in E. coli DnaJ. Both mutants resulted in the loss of Sec63 activity. On the basis of our structural model, these substitutions occur at the turn, from Y31 to D34 after helix II, discussed above. We cannot distinguish whether these mutations disrupt the turn and thus compromise the overall structure of DnaJ or physically disrupt the interface between the Hsp40 and Hsp70 preventing interaction.

A temperature-sensitive mutant of a different invariant residue in the J-homology region of Sec63 has been characterized by Nelson et al. (1993). This point mutation, A179T, results in severe secretion defects and may prevent interaction with Kar2p, the yeast DnaK homolog. It has been proposed that this mutation interrupts the hydrophobic face of one of the helices that interacts with Kar2p. On the basis of the data presented here, and that of Szyperski et al. (1994), it is probable that the corresponding mutation in DnaJ(1−78), A52T, would disrupt hydrophobic contacts with helix III. According to the ribbon model in Figure 4, however, the β-methyl of A52 packs into the hydrophobic core, and it appears that this mutation would result in unfavorable packing of DnaJ(1−78), not explicitly curtail an interaction with DnaK.

The structural model proposed here may give some insight into the structure of eukaryotic homologs involved in disease processes. Human MHC class II allele HLA DRB10401, an allele linked to patients with rheumatoid arthritis, contains sequence similarity with DnaJ although this homology is limited to a short stretch where seven out of nine amino acids are identical (Albani et al., 1992). In DnaJ, this region corresponds to K61−H70 near the C-terminus of DnaJ(1−78). In HLA DRB10401, this stretch is close to the putative peptide binding domain, which is proposed to be structurally related to the polypeptide binding pocket of Hsp70 proteins (Rippman et al., 1991). Even though the sequence similarity is over a very small region, antibodies raised against DnaJ in rabbits will bind to the HLA DRB10401 protein. It is interesting to note that in our structural model and that of Szyperski et al. (1994) this stretch of amino acids adopts an α-helical conformation. Given that the etiology of rheumatoid arthritis has been discussed in terms of shared epitopes between bacterial heat shock proteins and self-antigens that may be localized to the cell surface (Winfield & Jarjour, 1991), the structural information presented here may be useful in providing insight into this autoimmune disease.

ACKNOWLEDGMENT

We thank Dr. Julian Sturtevant at Yale for running the calorimetry analysis and value Kevin MacKenzie and Dr. Richard Kriwacki (currently at The Scripps Research Institute) for pulse sequence implementation as well as useful discussions. We also appreciate the help of Michael Andrec in analyzing the exchange data. J.M.F. was a member of Dr. Donald Engelman's laboratory, and we gratefully acknowledge his contributions of funding, laboratory space, and encouragement.

SUPPLEMENTARY MATERIAL AVAILABLE

Two figures from the 200-ms 3D NOESY-HMQC data set for residues S59 through G69 with one figure showing the sequential connectivities from the NH−Cα region and the other depicting the sequential connectivities from the NH−NH region, a table containing the ^{1}H and ^{15}N chemical shift data along with the $^{3}J_{HNH\alpha}$ values, and a table containing the short- and medium-range NOE connectivities observed in the 200-ms 3D NOESY-HMQC (12 pages). Ordering information is given on any current masthead page.

REFERENCES

Albani, S., Tuckwell, J. E., Esparza, L., Carson, D. A., & Roudier, J. (1992) *J. Clin. Invest. 89*, 327−331.

Andrec, M., Hill, R. B., & Prestegard, J. H. (1995) *Protein Sci.* (in press).

Bardwell, J. C., Till, A. K., Craig, E., King, J., Zylicz, M., & Georgopoulos, C. (1986) *J. Biol. Chem. 261*, 1782−1785.

Bax, A., & Davis, D. G. (1985) *J. Magn. Reson. 65*, 355−360.

Booker, G. W., Breeze, A. L., Downing, A. K., Panayotou, G., Gout, I., Waterfield, M. D., & Campbell, I. D. (1992) *Nature 358*, 684−687.

Bork, P. (1992) *Curr. Opin. Struct. Biol. 2*, 413−421.

Bork, P., Sander, C., Valencia, A., & Bukau, B. (1992) *Trends Biochem. Sci. 17*, 129.

Brünger, A. T. (1992) *X-PLOR Version 3.1*, Yale University Press, New Haven, CT.

Caplan, A. J., Cyr, D. M., & Douglas, M. G. (1993) *Mol. Biol. Cell 4*, 555−563.

Cheetham, M. E., Brion, J.-P., & Anderton, B. H. (1992) *Biochem. J. 284*, 469−476.

Englander, S. W., & Kallenbach, N. (1984) *Q. Rev. Biophys. 16*, 521−655.

Englander, S. W., & Mayne, L. (1992) *Annu. Rev. Biophys. Biophys. Chem. 21*, 243−265.

Feldheim, D., Rothblatt, J., & Schekman, R. (1992) *Mol. Cell. Biol. 12*, 3288−3296.

Flaherty, K. M., deLuca, C., & McKay, D. B. (1990) *Nature 346*, 623−628.
Georgopoulos, C. (1992) *Trends Biochem. Sci. 17*, 295−299.
Georgopoulos, C., & Welch, W. J. (1993) *Annu. Rev. Cell Biol. 9*, 601−634.
Gray, D. M., Lang, D., Kuner, E., Vaughan, M., & Sutherland, J. C. (1984) *Anal. Biochem. 136*, 247−250.
Griesinger, C., Otting, G., Wüthrich, K., & Ernst, R. R. (1988) *J. Am. Chem. Soc. 110*, 7870−7872.
Hartl, F. U., Hlodan, R., & Langer, T. (1994) *Trends Biochem. Sci. 19*, 20−25.
Hendrick, J. P., Langer, T., Davis, T. A., Hartl, F. U., & Wiedmann, M. (1993) *Proc. Natl. Acad. Sci. U.S.A. 90*, 10216−10220.
Hennessey, J. P., Jr., & Johnson, W. C., Jr. (1981) *Biochemistry 20*, 1085−1094.
Johnson, W. C., Jr. (1990) *Proteins: Struct., Funct., Genet. 7*, 205−214.
Kay, L. E., Marion, D., & Bax, A. (1989) *J. Magn. Reson. 84*, 72−84.
Kay, L. E., Keifer, P., & Saarinen, T. (1992) *J. Am. Chem. Soc. 114*, 10663−10665.
Kelley, W. L., & Georgopoulos, C. (1992) *Curr. Opin. Cell Biol. 4*, 984−991.
Kim, Y., & Prestegard, J. H. (1989) *J. Magn. Reson. 84*, 9−13.
Langer, T., Lu, C., Echols, H., Flanagan, J. M., Hayer, M. K., & Hartl, F. U. (1992) *Nature 356*, 683−689.
Leroux, P. (1988) *Proceedings of the Magnetic Resonance in Medicine, 7th Annual Meeting* (Raymond, A. E., Ed.) p 1049, Academic Press, San Diego.
Live, D. H., Davis, D. G., Agosta, W. C., & Cowburn, D. (1984) *J. Am. Chem. Soc. 106*, 1939−1941.
Marion, D., & Wüthrich, K. (1983) *Biochem. Biophys. Res. Commun. 113*, 967−974.
Marion, D., Driscoll, P. C., Kay, L. E., Wingfield, P. T., Bax, A., Gronenborn, A. M., & Clore, G. M. (1989a) *Biochemistry 28*, 6150−6156.
Marion, D., Kay, L. E., Sparks, S. W., Torchia, D. A., & Bax, A. (1989b) *J. Am. Chem. Soc. 111*, 1515−1517.
McKay, D. B. (1993) *J. Protein Chem. 44*, 67−98.
Morris, A. G., & Freeman, R. (1978) *J. Magn. Reson. 29*, 433.
Neidhardt, F. C., Bloch, P. L., & Smith, D. F. (1974) *J. Bacteriol. 119*, 736−747.
Nelson, M. K., Kurihara, T., & Silver, P. A. (1993) *Genetics 134*, 159−173.
Overduin, M., Rios, C. B., Mayer, B. J., Baltimore, D., & Cowburn, D. (1992) *Cell 70*, 697−704.
Patthy, L. (1991) *Curr. Opin. Struct. Biol. 1*, 351−361.
Richardson, J. S. (1981) *Adv. Protein Chem. 34*, 167−339.
Rippmann, F., Taylor, W. R., Rothbard, J. B., & Green, M. N. (1991) *EMBO J. 10*, 1053−1059.
Rowley, N., Prip-Buus, C., Westermann, B., Brown, C., Schwarz, E., Barrell, B., & Neupert, W. (1994) *Cell 77*, 249−259.
Shaka, A. J., Lee, C. J., & Pines, A. (1988) *J. Magn. Reson. 77*, 274−293.
Shinnar, M., Elff, S., Subramanian, H., & Leigh, J. S. (1989) *Magn. Reson. Med. 12*, 75−80.
Silver, P. A., & Way, J. C. (1993) *Cell 74*, 5−6.
Srivastava, P. K. (1993) *Adv. Cancer Res. 62*, 153−177.
States, D. J., Haberkorn, R. A., & Ruben, D. J. (1982) *J. Magn. Reson. 48*, 286−292.
Stuart, R. A., Cyr, D. M., Craig, E. A., & Neupert, W. (1994) *Trends Biochem. Sci. 19*, 87−92.
Studier, F. W., Rosenberg, A. H., Dunn, J. J., & Dubendorff, J. W. (1990) *Methods Enzymol. 185*, 60−89.
Sutherland, J. C., Desmond, E. J., & Takacs, P. Z. (1980) *Nucl. Instrum. Methods 172*, 195−199.
Sutherland, J. C., Keck, P. C., Griffin, K. P., & Takacs, P. Z. (1982) *Nucl. Instrum. Methods 195*, 375−379.
Szabo, A., Langer, T., Schroeder, H., Flanagan, J., Bukau, B., & Hartl, F. U. (1994) *Proc. Natl. Acad. Sci. U.S.A. 91*, 10345−10349.
Szyperski, T., Pellecchia, M., Wall, D., Georgopoulos, C., & Wüthrich, K. (1994) *Proc. Natl. Acad. Sci. U.S.A. 91*, 11343−11347.
Tolman, J. R., Chung, J., & Prestegard, J. H. (1992) *J. Magn. Reson. 98*, 462−467.
Vuister, G. W., & Bax, A. (1993b) *J. Am. Chem. Soc. 115*, 7772−7777.
Vuister, G. W., Clore, G. M., Gronenborn, A. M., Powers, R., Garrett, D. S., Tschudin, R., & Bax, A. (1993a) *J. Magn. Reson. 101B*, 210−213.
Waksman, G., Shoelson, S. E., Pant, N., Cowburn, D., & Kuriyan, J. (1993) *Cell 72*, 779−790.
Wall, D., Zylicz, M., & Georgopoulos, C. (1994) *J. Biol. Chem. 269*, 5446−5451.
Winfield, J., & Jarjour, W. (1991) *Immunol. Rev. 121*, 193−220.
Wüthrich, K. (1986) *NMR of Proteins and Nucleic Acids*, John Wiley, New York.
Zylicz, M., Yamamoto, T., McKittrick, N., Sell, S., & Georgopoulos, C. (1985) *J. Biol. Chem. 260*, 7591−7598.

BI9424656